Materials Science & Engineering C 117 (2020) 111311

Contents lists available at ScienceDirect

Materials Science & Engineering C

journal homepage: www.elsevier.com/locate/msec

Development of vascularized nerve scaffold using perfusion-decellularization and recellularization

Tsering Wüthrich[a,1], Ioana Lese[a,b,1], David Haberthür[c], Cédric Zubler[c], Ruslan Hlushchuk[c], Ekkehard Hewer[d], Louis Maistriaux[e], Pierre Gianello[e], Benoît Lengelé[e,f], Robert Rieben[a], Esther Vögelin[a,b], Radu Olariu[a,b,*,2], Jérôme Duisit[e,f,**,2], Adriano Taddeo[a,b,***,2,3]

[a] Department for BioMedical Research, University of Bern, Switzerland
[b] Department of Plastic and Hand Surgery, Inselspital, University Hospital, University of Bern, Switzerland
[c] Institute of Anatomy, University of Bern, Switzerland
[d] Institute of Pathology, University of Bern, Switzerland
[e] Institut de Recherche Expérimentale et Clinique (IREC), Université catholique de Louvain, Belgium
[f] Department of Plastic and Reconstructive Surgery, Cliniques Universitaires Saint-Luc, Brussels, Belgium

ARTICLE INFO

Keywords:
Vascularized nerve
Perfusion-decellularization
Extracellular matrix
Peripheral nerve injuries
Tissue engineering

ABSTRACT

Introduction: Vascularized nerve grafts (VNG) may offer an advantage in peripheral nerve regeneration by avoiding ischemic damage and central necrosis observed in non-VNG, particularly for the treatment of large and long nerve defects. However, surgical complexity, donor site morbidity and limited nerve availability remain important drawbacks for the clinical use of VNG. Here we explore the potential of perfusion-decellularization for bioengineering a VNG to be used in peripheral nerve reconstruction.

Methods: Porcine sciatic nerves were surgically procured along with their vascular pedicle attached. The specimens were decellularized via perfusion-decellularization and preservation of the extracellular matrix (ECM), vascular patency and tissue cytokine contents were examined. Scaffold reendothelialization was conducted with porcine aortic endothelial cells in a perfusion-bioreactor.

Results: Morphologic examination of decellularized VNG and analysis of the DNA content demonstrated cell clearance whereas ECM content and structures of the nerve fascicles were preserved. Using 3D micro-computed tomography imaging we observed optimal vasculature preservation in decellularized scaffolds, down to the capillary level. Cytokine quantification demonstrated measurable levels of growth factors after decellularization. Endothelial cell engraftment of the large caliber vessels was observed in reendothelialized scaffolds.

Conclusions: In this study we provide evidence that perfusion-decellularization can be used to create vascularized nerve scaffolds in which the vasculature and the ECM component are well preserved. As compared to non-vascularized conduits, engineered vascularized nerve scaffolds may represent an ideal approach for promoting better nerve regeneration in larger nerve defect reconstructions.

Abbreviations: 3D, three-dimensional; CPD, critically point dried; DAPI, 4′,6-diamidino-2-phenylindole; DDIC, digital differential interference contrast; dsDNA, double stranded DNA; ECM, extracellular matrix; FDA, Food and Drug Administration; H&E, hematoxylin and eosin; PBS, phosphate buffered saline; RT, room temperature; SD, standard deviation; SDS, sodium dodecyl sulfate; sGAG, sulfated glycosaminoglycan; TBS, Tris-buffered saline; VNG, vascularized nerve graft; VNG-ECM, decellularized vascularized nerve graft scaffolds; pVNG-ECM, decellularized porcine vascularized sciatic nerves; wtPAEC, wild type porcine aortic endothelial cells

* Correspondence to: R. Olariu, Department of Plastic and Hand Surgery, Inselspital Bern, Freiburgstrasse, 3010 Bern, Switzerland.
** Correspondence to: J. Duisit, UCL/SSS/IREC/CHEX, Avenue Hippocrate 55, mailbox B1.55.04, 1200 Brussels, Belgium.
*** Correspondence to: A. Taddeo, Institute of Virology and Immunology (IVI), Sensemattstrasse 293, 3147 Mittelhäusern, Switzerland.
E-mail addresses: radu.olariu@insel.ch (R. Olariu), jerome.duisit@uclouvain.be (J. Duisit), adriano.taddeo@ivi.admin.ch (A. Taddeo).
[1] These authors contributed equally to this work.
[2] These authors contributed equally as senior authors to this work.
[3] Current address: Institute of Virology and Immunology (IVI), Sensemattstrasse 293, 3147 Mittelhäusern, Switzerland.

https://doi.org/10.1016/j.msec.2020.111311
Received 4 December 2019; Received in revised form 15 July 2020; Accepted 25 July 2020
Available online 05 August 2020
0928-4931/

1. Introduction

Millions of people in Europe and United States of America suffer from traumatic nerve injuries every year with an estimated frequency of 1 in 1000 people in Europe. The incidence rate is especially high in the population of working adults [1]. Peripheral nerve injuries can have a tremendous impact on an individuals' life with negative effects ranging from psychological stress and social constraints to loss of functionality and, hence, invalidity [1]. Tension-free end-to-end suturing (i.e. nerve coaptation) is the preferred strategy for peripheral nerve repair. For short nerve gaps (0.5 cm) tension-free reconnection might not be practicable and a bridging nerve conduit might be necessary [2,3]. Autologous nerve grafts are the gold standard for repairing longer nerve gaps (> 1 cm). Although clinically effective, autologous nerve grafts come at a high cost for the individual due to donor site morbidity and the need for a second surgery site. Moreover, limited graft availability and mismatching nerve morphologies represent important drawbacks in the use of autologous nerve grafts [4].

In order to overcome these limitations, the fields of regenerative medicine and tissue engineering have produced a plethora of meaningful contributions on nerve tissue engineering and improved nerve grafts in the recent years [5]. Several types of nerve conduits consisting of a variety of materials have been developed and the translation of engineered nerve grafts to the clinic has been met with a certain degree of success [6]. Current tissue engineering approaches aim to generate nerve guidance conduits that could lead to the regeneration of the nerve by providing physical guidance for directing the sprouting axons as well as topographic, chemotactic and haptotactic cues that may lead to functional nerve regeneration [2]. The most promising candidates were found to be degradable collagen tubes and extracellular matrix (ECM) conduits [7]. In particular, the use of biological scaffold materials composed of ECM has proven to be effective, in part, because they provide native endogenous signals including optimal biological, biochemical and three-dimensional (3D) physiological environment [8]. Biological ECM nerve scaffolds are typically derived from processes that involve decellularization of the graft by using detergent-based decellularization applied in combination with agitation in order to eliminate the cellular component [9]. Recent preclinical studies have shown that decellularized ECM nerve scaffolds are superior to collagen conduits and perform equally to autografts and isografts [7], and therefore they may become an alternative in certain nerve reconstructions [9]. Currently, there is one FDA-approved decellularized nerve product on the market (Avance Nerve Graft, AxoGen). Clinical studies using this decellularized nerve from cadaveric source demonstrated promising results and improved performance and functionality due to the 3D architecture and the native ECM present in the grafts [10–12]. However, even though it has been suggested that decellularized ECM scaffold can be used to bridge large gaps (4–6 cm) [13,14], this technology has only been shown to be successful for the reconstruction of small diameters (1–2 mm) and short nerve gaps (< 3 cm) [7,12,14]. Due to this limitation of non-vascularized nerve grafts, autologous nerve graft remain the gold-standard for the reconstruction of larger nerves and longer gaps [3,15].

We have recently investigated the potential of perfusion-decellularization for the generation of tissue-engineered decellularized composite grafts, showing that this approach can be used to produce complex ECM scaffolds with a perfusable vascular tree and the potential for recellularization [16–18]. We speculate that the addition of a functional vascularization to tissue-engineered nerve conduits may be used to overcome the current limitations associated with the use of non-vascularized nerve conduits. It is known that vascularization plays an important role in nerve regeneration and that sufficient vascularization can support nerve repair and reconstruction (as recently reviewed in [19–21]). Vascularization can provide nutrients and oxygen to regenerate axons and associated cells, and thus promote cell survival and growth. It may also work as tracks for Schwann cell migration and sustains nerve regeneration by secretion of neurotrophic molecules from endothelial cells and blood-migrating cells. Vascularized nerve grafts (VNG) perform better than non-VNG and allow faster regeneration in certain clinical conditions such as large nerves, proximal lesions and non-vascularized recipient beds [19,21]. In this study, we aimed to develop a vascularized ECM nerve scaffold (VNG-ECM) using perfusion-decellularization, focusing on its preserved 3D and molecular structure as well as the anatomy and usability of its vascular tree for perfusion and recellularization.

2. Methods

2.1. Surgical technique for isolation of vascularized nerves

Seven porcine sciatic nerve grafts, along with their vascular pedicle, were surgically retrieved from wild-type pigs. Shortly after euthanasia, the pigs were placed in lateral decubitus and the hind limb was shaved and disinfected with Octenisept (Schülke & Mayr). A lazy-S incision was performed in the center of the proximal hind limb. After subcutaneous dissection and identification of the muscles, the biceps femoris muscle was disinserted from its distal attachment and everted posteriorly. The sciatic nerve, together with its two main branches (tibial and peroneal nerve), were carefully dissected and, under loupe magnification, the nutrient artery to the sciatic nerve was identified. This nutrient artery and its surrounding perivascular tissue were then traced back to its origin at the medial circumflex femoral artery. The dissection of the graft was carried out along the main pedicle proximally enough to reach arterial and venous calibers that were adequate for cannulation. After preparation of the pedicle, the entire specimen was harvested and then flushed through the artery with heparinized saline solution (5000 UI/100 ml saline) until clear fluid returned from the vein. Seven native nerves were taken from the fibular branch of the excised sciatic nerves to be used as controls. Vascularized sciatic nerves (n = 7) were weighed, measured and stored in phosphate buffered saline (PBS) supplemented with 2% penicillin/streptomycin (PS) at 4 °C until decellularization. Native fibular branches of the sciatic nerve (n = 7) were immediately processed and stored to be used as controls.

2.2. Perfusion-decellularization

Sciatic nerve grafts (n = 7) were prepared for perfusion-decellularization: the arterial pedicle was cannulated with a 14G catheter, and the venous pedicle was either left free or cannulated with a Luer. Grafts were immersed in a 500-ml glass jar, filled with PBS. The arterial pedicle was then connected to a peristaltic pump (Masterflex L/S, Cole-Palmer Instrument Co), via a 16G silicone tubing (Cole-Parmer). Perfusion flow was set from 3 to 3.5 ml/min, to ensure a mean arterial pressure below 100 mmHg. The following open-circuit perfusion sequence was applied, as previously determined, lasting a total time of 126,5 h through 7 steps: 1) 340 ml of normal heparinized (15 UI/ml) saline, with 10 μM adenosine (Sigma-Aldrich), at 4 °C, for 1.5 h; 2) 10,000 ml of 1% sodium dodecyl sulfate (SDS, VWR) in ultrapure water at room temperature (RT), for 50 h; 3) 870 ml of ultrapure water at RT, for 5 h; 4) 1300 ml of Triton-X 100 1% (VWR) in water at RT, for 5 h; 5) 10,000 ml of PBS at RT, for 50 h; 6) 1600 ml of type I Bovine DNAse (Roche I, Sigma-Aldrich), 50 UI/ml in PBS with 203.3 g/l magnesium chloride (Sigma-Aldrich), at 37 °C, for 12 h; 7) 630 ml of final PBS wash, at RT, for 3 h. Decellularized porcine vascularized sciatic nerves (pVNG-ECM) were stored at 4 °C in PBS until further processing.

2.3. Fluoroscopy

The patency of the vascular pedicle, as well as the branching of the perforators supplying the nerve, were confirmed in the isolated nerves before (n = 7) and after decellularization (n = 7) through fluoroscopy by using Iobitridol (Xenetix 300 mg/ml, Guerbet AG) as contrast agent.

2.4. DNA quantification

DNA was extracted from native (n = 6) and decellularized (n = 7) biopsies (average wet weight 22.4 ± 3.8 mg and 21.1 ± 2.8 mg, respectively) using a commercial kit (DNeasy Blood & Tissue Kit, Qiagen) according to the manufacturer's instructions for tissue samples. DNA quantification was performed with a QuantiFluor dsDNA Sample Kit (Promega) according to the manufacturer's instructions. Fluorescence intensity of the intercalating agent was measured on a plate reader (Tecan Reader Infinite M1000, Tecan) at $504nm_{Ex}/531nm_{Em}$.

2.5. Histology

With a single transversal cut a section of approximately 8 mm thickness of each native nerve (n = 7) or pVNG-ECM (n = 7) was severed and immediately fixed in formaldehyde followed by paraffin-embedding. Slides were stained with hematoxylin and eosin (H&E) and scanned on a Pannoramic 250 Flash ii scanner (3DHISTECH, Budapest, Hungary) in order to enable digital analysis. Slide observation, evaluation of histoarchitecture and structure preservation were carried out in the digital slide manager program CaseViewer 2.1 for Windows (3DHISTECH).

2.6. Immunofluorescence

Pieces of the native nerves (n = 7) and pVNG-ECM (n = 7) nerve scaffolds were embedded in Tissue-Tek O.C.T. Compound (Sakura Finetek US Inc.) for immunofluorescence staining. Fine transversal sections of 6 µm were cut on a HYRAX C 60 (Zeiss) cryostat. For the immunofluorescence staining of the native and decellularized tissues the slides were air dried at room temperature, fixed in acetone and rehydrated in Tris-buffered saline (TBS). Subsequently the staining area was confined with Dako-pen (Dako; cat. no. S 2002) and incubated in a blocking solution of TBS-PBS-3% BSA for 1 h at room temperature. Then the slices were rinsed with TBS and the primary antibodies (diluted in TBS-PBS-1% BSA solution) were applied and incubated overnight at 4 °C. The following primary antibodies were used: rat anti-porcine CD31 (MAB33871, clone 377537, 1:200, R&D systems), rabbit anti-collagen IV (ab6586, polyclonal, 1:50, Abcam) and rabbit anti-laminin (ab11575, polyclonal, 1:50, Abcam). The following day, the slides were extensively washed with TBS to remove unbound antibodies before application of 4′,6-diamidino-2-phenylindole (DAPI) and the secondary antibodies in TBS-PBS-1% BSA for one and a half hours at room temperature. The following secondary antibodies were used as necessary: goat anti-rat IgG Alexa488 (3010-02, Southern Biotechnology), goat anti-mouse Alexa488 (1082-08, Life Technologies) and goat anti-rabbit IgG FITC (4050-02, Southern Biotechnology). After extensive washing, the slides were mounted with a drop of pre-warmed glycergel (C0563, Dako) and immunofluorescence pictures were taken on a Leica DMI4000 B fluorescence microscope (Leica Microsystems). Quantification of fluorescence intensity was carried out in ImageJ Version 1.49 (National Institutes of Health, [22,23]) as described previously [24].

2.7. Quantification of sulfated glycosaminoglycan

Sulfated glycosaminoglycan (sGAG) content of the native (n = 7) and decellularized (n = 7) nerve scaffolds was quantified using a commercially available kit (Glycosaminoglycan Assay, Blyscan). All steps were performed according to the manufacturer's instructions. Samples were transferred in duplicates onto a flat-bottom transparent 96-well plate suitable for optical density measurements. Absorption was measured at 656 nm on a plate reader (Tecan Reader Infinite M1000, Tecan).

2.8. Micro-computed tomography (micro-CT)

2.8.1. Sample preparation

pVNG-ECM (n = 2) were instilled with µAngiofil [25] obtained from Fumedica AG (Muri, Switzerland) using the cannulated artery. After instillation, the samples were stored in 2% PFA prior to scanning. In a first round, samples were scanned immersed in the liquid. In order to perform high-resolution imaging, after the first scan, one pVNG-ECM was dissected and one part of it was dehydrated in a graded ethanol series and critically point dried (CPD) with a Leica EM CPD300 according to a standard protocol.

2.8.2. Imaging

All samples were imaged on a Bruker SkyScan1272 high resolution microtomography scanner (Bruker microCT) as previously described [25]. Depending on the scanning modalities (i.e., low or high resolution for wet and critically dried samples, respectively) different scanning parameters were set as specified below.

Low resolution scanning of the pVNG-ECM was performed by setting the X-ray source to a voltage of 100 kV and a current of 100 µA. A 0.11 mm thick Copper filter was used to shape the spectrum of the X-ray source. A set of 471 projections of 1224 × 820 pixels at every 0.4° over 180° were acquired with each projection exposed for 2899 ms. Five projections were averaged to one to reduce noise. This resulted in a scan time of about 2 h and an isometric voxel size of 21.8 µm in the final datasets.

High resolution scanning for the CPD sample was performed with the X-ray source set to a voltage of 60 kV and a current of 166 µA. A 0.25 mm thick aluminum filter was used to shape the spectrum of the X-ray source. A set of 962 projections of 2452 × 1640 pixels at every 0.2° over a 180° sample rotation were acquired with every projection exposed for 1114 ms. Four projections were averaged to reduce noise. This resulted in a scan time of about 1.5 h and an isometric voxel size of 8 µm in the final datasets.

The projection images were then subsequently reconstructed into a 3D stack of images with NRecon (Bruker, Version: 1.7.0.4).

2.9. Cytokine analysis

Total protein from native (n = 7) and decellularized (n = 7) tissue (average biopsies wet weight 209.7 ± 105.7 mg) was extracted as described before [17,18]. For cytokine and growth factor analysis two different Luminex-type protein detection assays were used: a multiplex specific for human nerve growth factor (EPX110-12170-901, ProcartaPlex, Thermo Scientific) and a homemade porcine-specific multiplex immunoassay [26]. The procedures were held according to the manufacturer and previously published instructions [26]. Sample acquisition was performed on the FlexMap3D system (Bio-Rad). Extrapolated values obtained from the 5PL logistic curve were included in the analysis, concentration values that cannot be extrapolated were considered out-of-range and excluded. Analyte levels were normalized to the initial mass of the biopsies and displayed as pg protein per mg of tissue.

2.10. Porcine aortic endothelial cell culture

Wild type porcine aortic endothelial cells (wtPAEC) were isolated and expanded in Dulbecco's Modified Eagle Medium (DMEM) supplemented with 10% fetal bovine serum (FBS) and 1% PS at 37 °C, 5% CO_2 [27]. After isolation, cells were cultured in chamber slides and characterized for the expression of CD31 and VE-cadherin as previously described [27,28]. Cultures with > 95% expression of endothelial markers were expanded (up to the 6th passage) and used for the recellularization experiments. Before seeding into the pVNG-ECM for recellularization, wtPAEC were fluorescently labeled by a membrane staining (PKH26 Red Fluorescent Dye Kit, PKH26GL, Sigma-Aldrich)

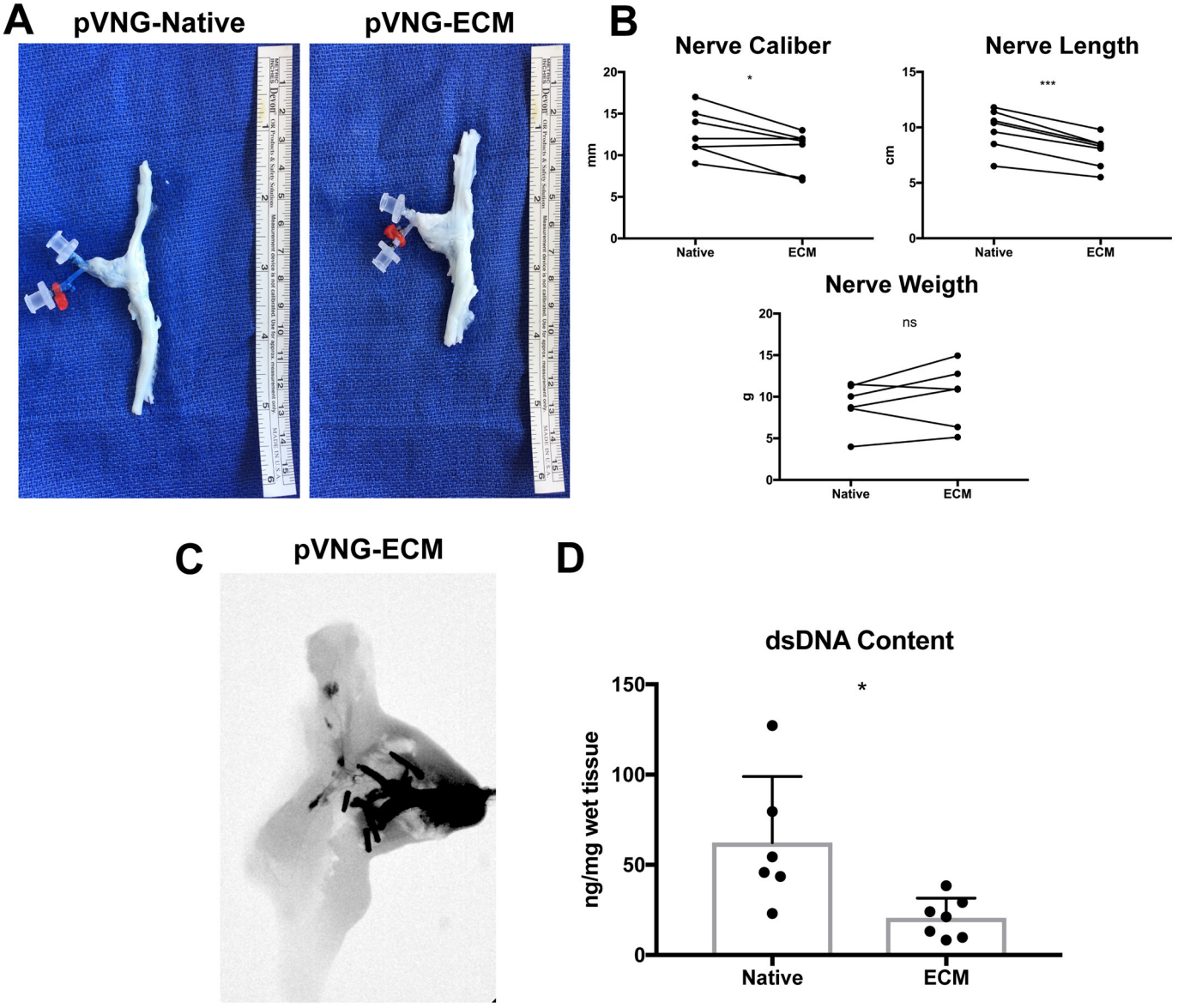

Fig. 1. Perfusion decellularization of porcine vascularized nerve grafts (pVNG). A) Native pVNG with its vascular pedicle cannulated and prepared for decellularization and pVNG-extracellular matrix (ECM) scaffold after decellularization. One image representative of seven pVNG. B) Nerve caliber, length and pVNG weight before and after decellularization. Each line represents the native pVNG and its decellularized (ECM) counterpart. ns = not significant, * $p < 0.05$, *** $p < 0.001$ by 2-tailed unpaired *t*-test. C) Arterial fluoroscopy of decellularized pVNG, (one image representative of seven). D) Double- strand DNA (dsDNA) content in native versus decellularized (ECM) pVNG, expressed in ng/mg wet weight. Data presented as individual values (n = 6 for native-pVNG and n = 7 for ECM-pVNG) and mean ± SD. *$p < 0.05$ by unpaired student *t*-test.

following the manufacturer's instruction.

2.11. Recellularization of the nerve scaffolds

Recellularization experiments were conducted in a specifically designed bioreactor. The arterial catheter of the decellularized scaffold was connected to a peristaltic pump – Minipuls 3 with 8 channels (Gilson, Villiers le bel, France) – via sterile silicone tubing with stoppers (Gilson) and extension silicone tubings (Gobatec, Bern, Switzerland) and immersed in a 500 ml glass jar filled with the same solution as the one used for the perfusion. Perfusion was performed in an open circuit fashion (i.e., outlet from scaffold into the jar and from the jar to the scaffold) (Supplementary Fig. 1) at a constant flow rate of 2 ml/min. First, decellularized nerve scaffolds (n = 3) were sterilized by continuous perfusion under physiologic conditions with 0.1% peracetic acid in PBS for 4 h followed by 4 h of washing with sterile PBS. Conditioning of the scaffold was also performed under constant perfusion with pure DMEM culture medium at 37 °C and 5% CO_2 overnight. The following day, the condition medium was removed and the VNG-ECM disconnected from the perfusion system and wtPAEC were injected into the vascular tree via the arterial cannula in four consecutive injections of 2.5×10^6 cells over the course of 2 h (i.e., 2.5×10^6 cells every half an hour, for a total of 1×10^7 cells). The perfusion system was reconnected to the arterial cannula and the flow slowly applied. Starting from 0.5 ml/min the flowrate was increased every half an hour up to 2 ml/min. This bioreactor was incubated under normal conditions at 37 °C, 5% CO_2 and fresh medium (DMEM supplemented with 10% FBS and 1% PS) was added every second to third day. Vessel reconstitution was monitored non-invasively using a Nikon Eclipse Ti-E Spinning Disk microscope (Nikon) and analyzed with NIS-Elements (Nikon) at days 0, 1 and 7. At the end of the experiment, samples were collected and analyzed by immunofluorescence as described above.

2.12. Statistical analysis

Graphic presentation and statistical analysis were performed with Prism 7 (GraphPad Software). Paired *t*-test was performed to compare the caliber, length and weight of the grafts before and after decellularization. Other comparisons between native and decellularized graft samples were conducted with unpaired student *t*-tests. For cytokines, multiple t-tests with Holm-Sidak correction were performed to quantitatively compare their abundance in native and decellularized tissues. One-way ANOVA with post-hoc Tukey's multiple comparison correction was used to compare the relative preservation of the different cytokine groups within the analyzed tissues. Data are presented as mean ± standard deviation (SD). $p < 0.05$ was considered statistically significant.

3. Results

3.1. Macroscopic assessment of decellularized porcine vascularized nerve grafts (pVNG-ECM)

After completion of the final perfusion-decellularization step, the produced pVNG-ECM scaffold demonstrated a preserved macroscopic structure (Fig. 1A). pVNG-ECM length and nerve-caliber were significantly reduced as compared to native grafts (caliber: 10.61 ± 2.42 mm and 12.71 ± 2.75 mm, $p = 0.019$; length: 7.89 ± 143 cm and 9.83 ± 1.83 cm, $p = 0.023$, mean ± SD respectively) while the weight did not change significantly (10.17 ± 3.75 g and 9.03 ± 2.75 g, respectively) (Fig. 1B). The preserved morphology of the nerve scaffold and its acellular pedicle allowed its handling and the use of the cannulated artery for analyzing internal vascularization of pVNG-ECM by fluoroscopic angiography. All the pVNG-ECM showed a perfusable vascular tree inside the nerves (Fig. 1C and Supplementary Video 1). Double strand DNA (dsDNA) content in pVNG-ECM was 20.6 ± 11 ng/mg wet weight compared to 62.3 ± 36.7 ng/mg wet weight in native samples with a 67% DNA reduction in decellularized scaffolds ($p = 0.015$) (Fig. 1D).

3.2. Histological evaluation

H&E staining revealed that pVNG-ECM maintained their tissue architecture and bundle-like structures after perfusion-decellularization with an overall structure that closely resemble the one of native grafts (Fig. 2A). Notably, decellularized nerve channels showed complete loss of myelinated fibers and nuclei, whereas the surrounding layers of connective tissue still showed some remaining nuclei. In contrast, untreated controls displayed a normal density of myelinated fibers and morphologically intact myelin sheaths.

To further confirm cell clearance, we performed a nuclear staining using DAPI and an endothelial cell staining using the CD31 marker. In agreement with the H&E finding, nucleated cells and CD31 were completely absent in p-VNG-ECM (Fig. 2B).

3.3. Vascular imaging

Micro-CT scanning was performed in order to obtain a detailed visualization of the vascular tree in the decellularized scaffolds. VNG-ECM revealed optimal vasculature preservation with a ramified, fully patent framework down to the capillary level (Fig. 3A, Supplementary Video 2). Some leakage points were observed. Analysis of critical point dried scaffold with high-resolution scanning and microtomographic reconstruction allowed 3D visualization of the patent vessels confirming the preservation of the nerve structure and of both the extrinsic system, along the surface of the decellularized peripheral nerve, and the intrinsic system, in the inner endoneural compartment (Fig. 3B and Supplementary Video 3).

3.4. Evaluation of the extracellular matrix

Immunofluorescence staining for collagen type IV and laminin showed that the perineurium was well preserved in all the pVNG-ECM (Fig. 4A). The basal lamina of the single fibers was preserved to a certain extent, but it appeared to be collapsed and not well organized. Quantification of the fluorescence intensity of these markers showed a significant reduction in decellularized scaffold as compared to native tissue with 62.90% and 38.14% preservation of collagen type IV and laminin respectively (Raw Integrated Density collagen IV: 40218990 ± 10,218,719 and 63,942,835 ± 10,385,614, $p = 0.001$; laminin: 25630076 ± 8,023,040 and 67,208,861 ± 13,630,931 $p < 0.0001$ for decellularized and native scaffolds, respectively) (Fig. 4B). Quantification of sulfated glycosaminoglycans content in the pVNG-ECM showed no significant decrease in decellularized scaffolds as compared to native tissue (4.44 ± 2.95 μg/mg and 4.88 ± 4.13 μg/mg dry tissue, respectively, Fig. 4C).

3.5. Cytokine preservation

Two multiplex assays (a 11-Plex Human ProcartaPlex and a homemade porcine inflammatory multiplex assay) were carried out to assess the levels of neurotrophic, inflammatory and complement factors in pVNG-ECM with respect to their native counterparts. As shown in Table 1, of the 19 cytokines measured ten presented detectable levels in native tissue. Most of these cytokines were detectable also in decellularized scaffold, with the exception of MCP-1 that was undetectable (Table 1). Of the other nine detectable cytokines four presented a significant reduction in pVNG-ECM as compared to native tissues (i.e., PIGF-1, BDNF, FGF-2 and sC5b-9, Table 1).

3.6. Recellularization experiments

Considering the presence of growth factors, perfusable vascular tree and good ECM preservation in decellularized scaffolds, we assessed the possibility of re-endothelialization of the pVNG-ECM using primary wtPAEC. Recellularization experiments using a specifically designed bioreactor showed that fluorescence labeled wtPAEC injected in pVNG-ECM and cultured under perfusion settled inside the vessels, and vessel-like structures were visible inside the nerve 7 days after injection (Fig. 5A). Immunofluorescence staining using CD31 and DAPI on day 7 confirmed that CD31 positive cells attached and aligned along the decellularized, bigger caliber vessels close to the pedicle (Fig. 5B to be compared with the pVNG-ECM of Fig. 2B). However, very few cells could be observed at more distal parts of the scaffold at this time point.

4. Discussion

Here we describe a model of vascularized ECM nerve graft (VNG-ECM) generated using perfusion-decellularization and evaluate its morphological and vascular properties as well as its recellularization potential. Our results offer several insights and suggestions for the generation of VNG-ECM at a clinical scale. In our study we focused on a large and long nerve such as the sciatic nerve, because we think that this kind of graft may help to overcome the current limitations associated with autologous and conduit-based nerve grafting.

A pig model was chosen because we have previously shown its relevance to size decellularization experiments and apparatus at a preclinical scale as well as its predictivity for the use of elderly postmortem human samples, even several days after death [16,18]. We showed that retrieval of nerve with an accessible vascular pedicle could be performed with a relatively simple surgical protocol. Importantly, vascular tree patency was displayed in all the collected nerve grafts. It is important to highlight that the collection of only partially vascularized grafts can compromise perfusion and thus success in the decellularization process. This encourages the use of angiographic techniques at

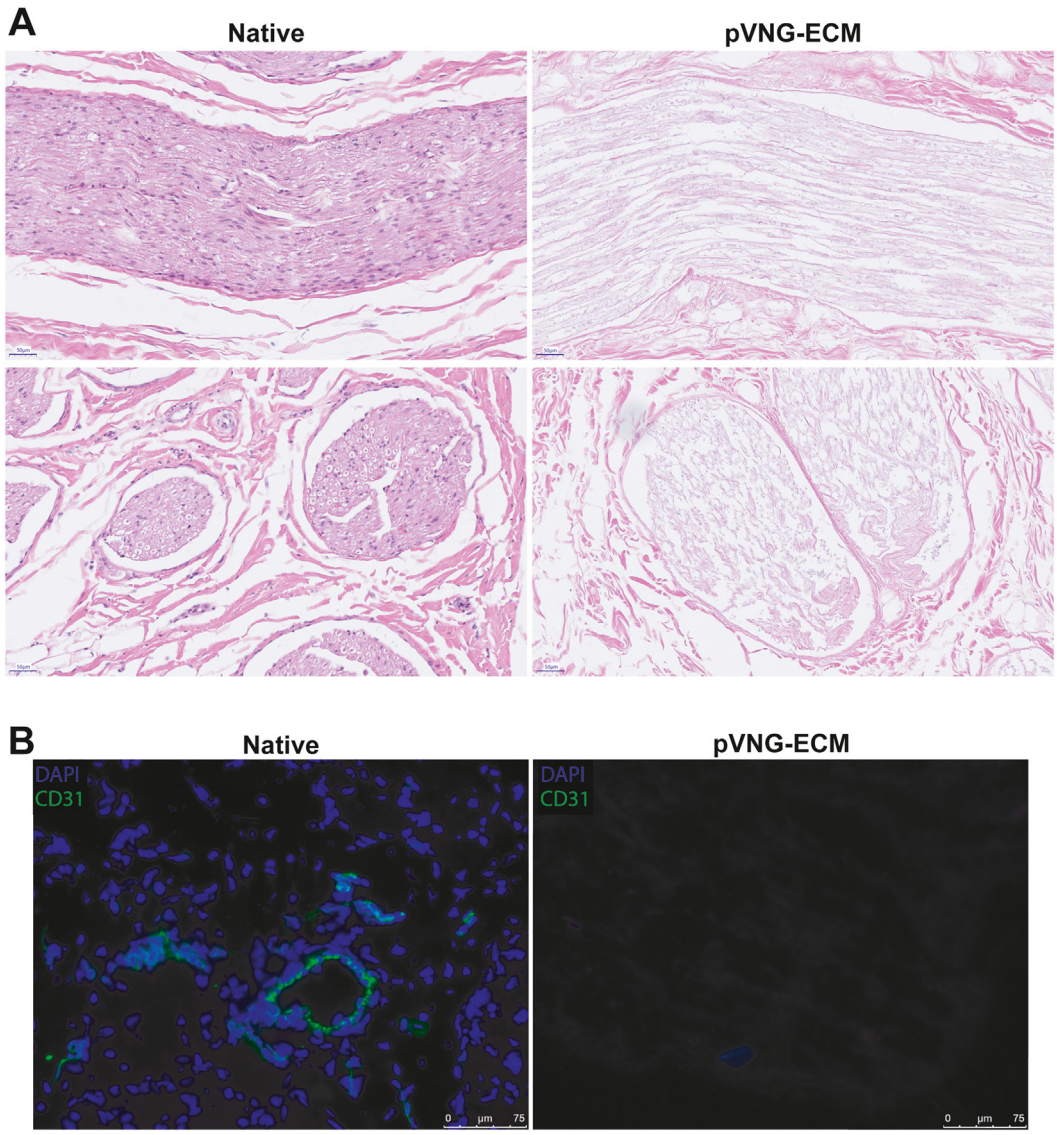

Fig. 2. Histological evaluation and cell removal in porcine vascularized nerve grafts (pVNG). A) Representative hematoxylin and eosin (H&E) staining comparing native (left) and decellularized (right) pVNG (n = 7 native and n = 7 decellularized). The upper row shows a transversal section (20× magnification) while the lower row shows a longitudinal section (20× magnification) of native and decellularized pVNG. B) Anti-CD31 (green) and DAPI (blue) staining showing native (left) and decellularized (right) pVNG sections (representative of n = 7 native and n = 7 pVNG-ECM). (For interpretation of the references to colour in this figure legend, the reader is referred to the web version of this article.)

the moment of graft collection to ensure the retrieval of a nerve conduit with its perfusable vascular pedicle and, therefore, an accurate perfusion territory that could be more efficiently decellularized. Indeed, although VNG-ECM showed no remaining nuclei both by DAPI-staining and histological analysis, we observed some nucleic acid in the dense connective tissue surrounding the nerve. This suggests that decellularization might have disrupted but not completely removed DNA contents in the connective tissue, as reported for other commercial decellularized products [29]. Notably, our native dissected grafts presented more remaining external connective tissue than other studies of decellularized nerve grafts. The DNA content of these native nerves was highly dispersed (20.6 ± 11 ng/mg wet weight), suggesting a heterogeneous cell content in the retrieved nerves. A more precise removal of the connective tissue can reduce variability and residual DNA content of VNG-ECM. Moreover, the addition of an orbital agitation bath during the SDS step may ensure a complementary decellularization of non-perfused areas. Additionally, decellularization treatment, and in particular endonuclease treatment, should be implemented to successfully reduce the dsDNA content. Several recent reports have compared the effects of different detergents/enzymes and treatment duration [30–32]. Further studies in this direction are warranted to assess the best decellularization and DNase protocol for the preparation of vascularized nerve scaffolds [32]. This treatment should bring dsDNA content under the threshold indicated by current decellularization guidelines (i.e., 50 ng dsDNA/mg ECM) [33] and the guidelines published by the World Health Organization (WHO) and US Food and Drug Administration (FDA) [34,35] which recommend < 10 ng residual cellular DNA per parenteral dose [36].

As shown for other tissues [17,18], we confirm that the nerve ECM structural components and 3D organization are well preserved following perfusion-decellularization. The sulfated glycosaminoglycan content did not change significantly, and histological analysis and laminin and collagen IV staining showed that the perineurium and the nerve honeycomb structures were maintained in VNG-ECM. These results demonstrate that perfusion-decellularization is a feasible approach for generating peripheral nerve scaffolds similarly to what has been demonstrated for other tissues [37]. Additionally, although it has been reported that SDS treatment can have a deleterious effect on certain

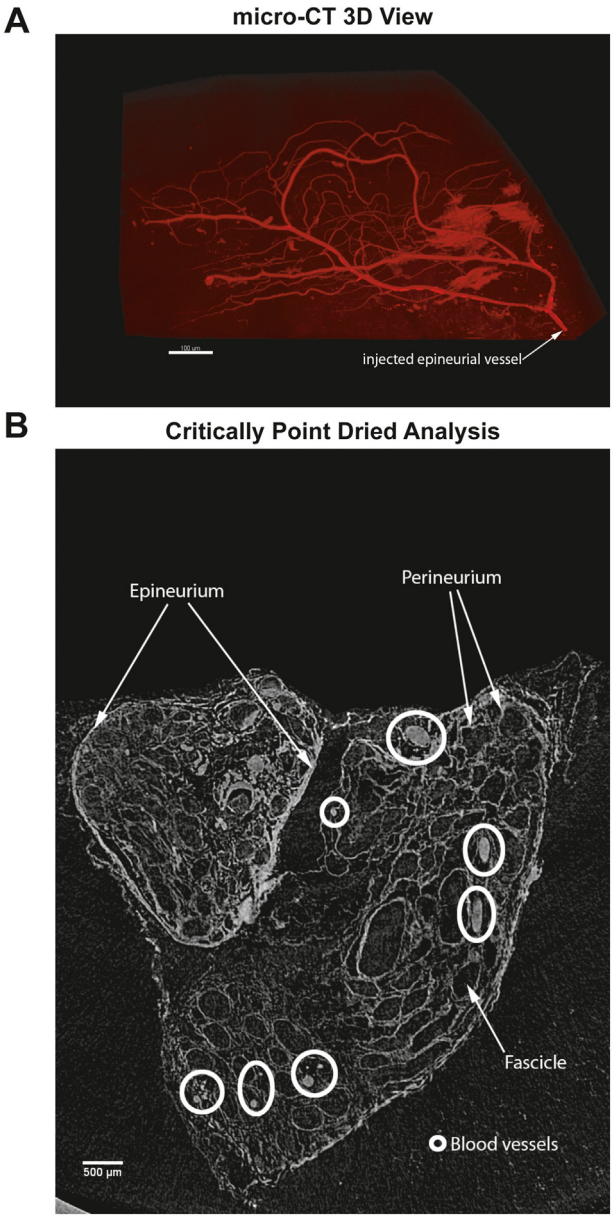

Fig. 3. Evaluation of the vascular tree in porcine vascularized nerve grafts (pVNG). A) Micro-computer tomography (micro-CT) of decellularized pVNG (representative of two visualizations). The artery of the vascular pedicle was injected with µAngiofil contrast agent and 3D reconstruction performed. B) High-resolution visualization of a critical point dried scaffold after µAngiofil-injection. Nerve honeycomb structure is visible with its epineurium and perineurium. Vessels are clearly visible due to the injection of the contrast medium. Instillation artifacts were removed and they are visible in the Supplementary Videos 2 and 3.

ECM components when used at high concentrations and long incubation time [38], our study confirms that the combined 1% SDS and Triton X-100 decellularization method is an efficient way to produce peripheral nerve allograft scaffolds [30,39]. Indeed, as compared to previously reported data [16–18], we observed a very high preservation of sGAG in VNG-ECM. GAG are known to interact with growth factors and neurotrophic factors involved in neural migration, axon guidance and neurite outgrowth and can either act as a barrier to axon growth or promote neural adhesion, migration and neuritogenesis [40]. In this process, the sulfation patterns of GAG chains seem to directly influence the binding of the proteoglycan to active proteins [40]. Further studies are warranted to characterize the motifs present in VNG-ECM proteoglycans in order to understand their capacity to fine-tune the microenvironment to promote rather than inhibit nerve regeneration.

Importantly, axonal regrowth requires a number of intrinsic and extrinsic factors as well as a permissive microenvironment [41]. A large number of neurotrophic factors are utilized in tissue engineering to improve peripheral nerve regeneration and the most potent mediators include brain-derived neurotrophic factor (BDNF), nerve growth factor (NGF) and the vascular endothelial growth factor (VEGF) family [42]. These neurotrophic factors have been successfully incorporated in different systems and their capacity to promote axonal regeneration has been reported in several pre-clinical models [42,43]. Our study shows that after perfusion-decellularization, all the ten measurable growth factors, were still detectable in decellularized although at decreased levels. Although the study was not designed to evaluate the significance and the bioactivity of these cytokines, it has been previously demonstrated that growth factors such as VEGF and bFGF are present in acellular ECM scaffolds and retain their biological activity following decellularization [44–47], suggesting that these growth factors may contribute to promote cellular growth and nerve regeneration in VNG-ECM scaffolds. The functionalization of the scaffold by additionally providing important neurotrophic factors, such as BDNF and NGF, may be used to increase nerve regeneration [42].

When compared to other nerve guidance channels, the most important aspect of our scaffold is the presence of a preserved vasculature. In order to better characterize the structure of this network, we used a microCT imaging approach in combination with the novel polymerizing contrast agent µAngiofil to visualize the scaffold vasculature in its entirety [25]. Thanks to this detailed tomographic 3D visualization, we could demonstrate that pVNG-ECM maintained the hierarchical structure and geometrical complexity of the vascular tree down to the capillary level. Some leakage was observed in the scaffold. Most likely, this is the result of a high, over-physiological injection-pressure of the contrast medium as previously discussed [25]. However, it is important to underline that special care should be taken to keep the perfusion pressure as uniform as possible during perfusion-decellularization and in any further perfusion-step to avoid disruption of the vascular network. Notably, high-resolution visualization of critical point dried scaffolds after µAngiofil-injection into the vascular pedicle confirmed the integrity of the nerve structure with its intrinsic and extrinsic blood supply.

A functional vascular network is the sine qua non for successful in vivo implantation of complex bioengineered tissue provided with a vascular pedicle [48]. Considering that in our model vasculature is the main strategy for improving nerve regeneration, we believe that the first endpoint of recellularization strategies for VNG-ECM should be the regeneration of the vascular compartment in order to allow long term, thrombosis-free implantation by covering collagen present on the basal lamina which may come into contact with circulating platelets to activate the coagulation cascade. In our attempts to reendothelialize the scaffold, we obtained a diffuse cell engraftment in the proximity of the vascular pedicle used for cell injection. These results support the experiment's goal to show the biocompatibility of the scaffold and the capacity to sustain endothelial cell lining. However, recellularization of microvasculature and capillary beds in the distal part of the nerve was not observed in these pilot experiments, and this is critical for understanding how we should proceed to recellularize in the future. We used only a limited number of cells for the recellularization experiments and it is likely that more cells will be needed to cover the entire vascular structure including also smooth muscle cells and pericytes to further support vessel reconstitution and control vessel permeability. Moreover, recellularization from both arterial and venous conduits, as well as injections in the nerve may lead to more homogenous cell distribution and significantly higher coverage, as shown for lung re-endothelialization [48]. Finally, the cells used were porcine aortic endothelial cells, thus originating from the biggest vessel in the porcine body. The use of organ and vessel-specific endothelial cells may show

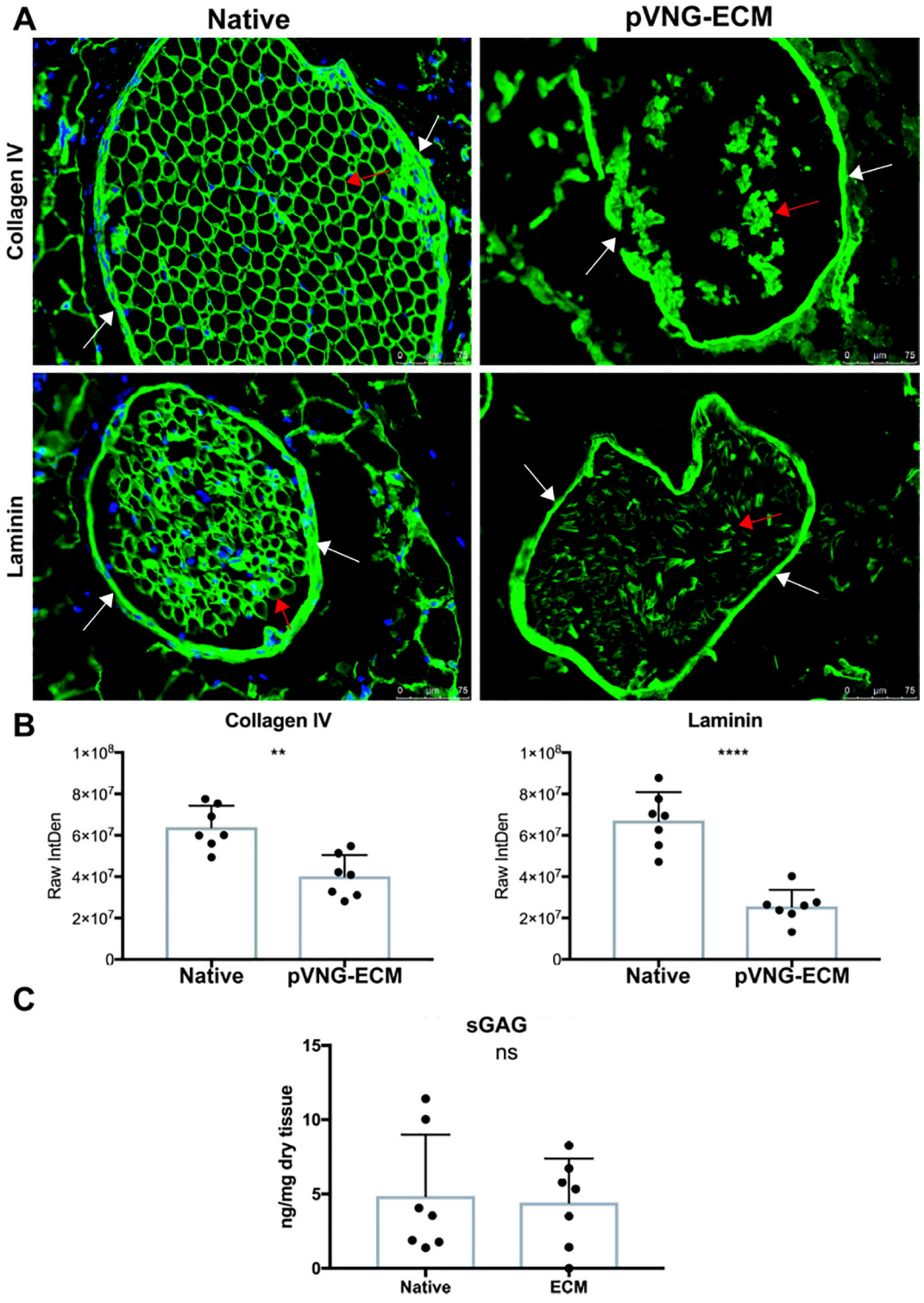

Fig. 4. Extracellular Matrix (ECM) evaluation in porcine vascularized nerve grafts (pVNG). Representative immunofluorescence images of collagen IV (green, upper row), laminin (green, lower row) and DAPI (blue) comparing native (left, n = 7) and decellularized (right, n = 7) pVNG. White arrows indicate the perineurium and red arrows the endoneurium. B) Quantification of the immunofluorescence signal (expressed as Raw integrated Density) of collagen IV and laminin staining in native and decellularized nerves. C) Quantification of sulfated glycosaminoglycan (sGAG) content in native (n = 7) and decellularized (n = 7) pVNG. Data presented as individual values (n = 7 for native-pVNG and n = 7 for ECM-pVNG) and mean ± SD. ns = not significant, *p < 0.05, **p < 0.01 by unpaired student t-test. (For interpretation of the references to colour in this figure legend, the reader is referred to the web version of this article.)

greater potential in generating a uniformly reendothelialized vascular tree [49,50]. We speculate that VNG-ECM may be successfully implanted once the vascular compartment is fully regenerated and then the regeneration of the nerve will be completed in vivo, where nerve regeneration will be sustained and promoted by the better nutrient and oxygen supply guaranteed from the vascularized grafts.

Table 1
Cytokine quantification in porcine vascularized nerve grafts (pVNG). Cytokine measurements analyzed by Luminex-like multiplex assay. Mean protein picogram abundance per milligram of tissue, standard deviation (SD), N values and the relative preservation in the decellularized pVNG-ECM with respect to native-pVNG are reported. *Adjusted p value calculated by multiple *t*-tests with Holm-Sidak correction. Bold values denote statistical significance at the $p < 0.05$ level. n.d. Not determined.

	Native			ECM			Comparison	
	Mean (pg/mg tissue)	SD	N	Mean (pg/mg tissue)	SD	N	Adjusted P value*	Mean preservation (%)
PIGF-1	0.0143	0.0062	7	0.0025	0.0013	7	**0.0062**	17.14
BDNF	0.0139	0.0071	7	0.0025	0.0014	7	**0.0209**	17.62
FGF-2	2.6012	1.7787	7	0.0936	0.0448	7	**0.0424**	3.60
VEGF-A	0.0288	0.0107	7	0.0126	0.0066	7	0.0703	43.80
IL1-beta	0.0862	0.0720	7	0.0275	0.0194	7	0.4575	31.94
IL-6	0.1875	0.1712	7	0.0248	0.0154	7	0.2863	13.25
MCP-1	0.1045	0.0416	7	Under detection range			n.d.	n.d.
C5a	0.0533	0.0458	7	0.0164	0.0124	7	0.4575	30.77
sC5b-9	0.0152	0.0076	7	0.0021	0.0013	7	**0.0123**	13.58
IL-10	0.3731	0.2900	7	0.0839	0.0652	7	0.2742	22.50

5. Conclusion

In this study we provide evidence that perfusion-decellularization can be used to create vascularized nerve scaffold in which the vasculature and the ECM component are well maintained. This holds great promise for generating better scaffolds for peripheral nerve reconstruction. These VNG-ECM may be generated from animals – for example genetically modified pigs to reduce antigenicity – or cadaveric human donors, increasing graft availability and possibilities to match nerve morphologies to create customized nerve scaffolds for specific lesions also with multiple vascular pedicles. Importantly, we showed that VNG-ECM have the potential to be reendothelialized in vitro in specifically designed bioreactors. The goal of future experiments should be to improve the efficiency of recellularization by enhancing density and engraftment of vascularly seeded cells, in order to produce fully reendothelialized scaffolds. Although VNG-ECM will be more complex to implant as compared to non-vascularized grafts, we hypothesize a benefit of vascularized nerve grafts over non-vascularized alternatives in longer nerve defects. To test this, it will be necessary to conduct in vivo studies assessing the efficacy of VNG-ECM for the repair of different kinds of peripheral nerve injuries, evaluating their advantages as compared to non-vascularized conduits.

Supplementary data to this article can be found online at https://doi.org/10.1016/j.msec.2020.111311.

Author contributions

TW performed all the scaffold evaluations, seeding experiments and prepared a first version of the manuscript. IL and RO designed the surgical model and were responsible for specimen collection and wrote the respective methods. DH, CZ and RH performed the microCT-scanning and critically point dry experiment and analyzed the respective data. EH performed all histological processing and evaluation. LM participated to graft preparation and scaffold production. PG, BL, RR and EV participated in study design, data interpretation and provided experimental support and funding. JD designed the study and performed all decellularization experiments and revised manuscript extensively. AT designed study, interpreted data, wrote the article and

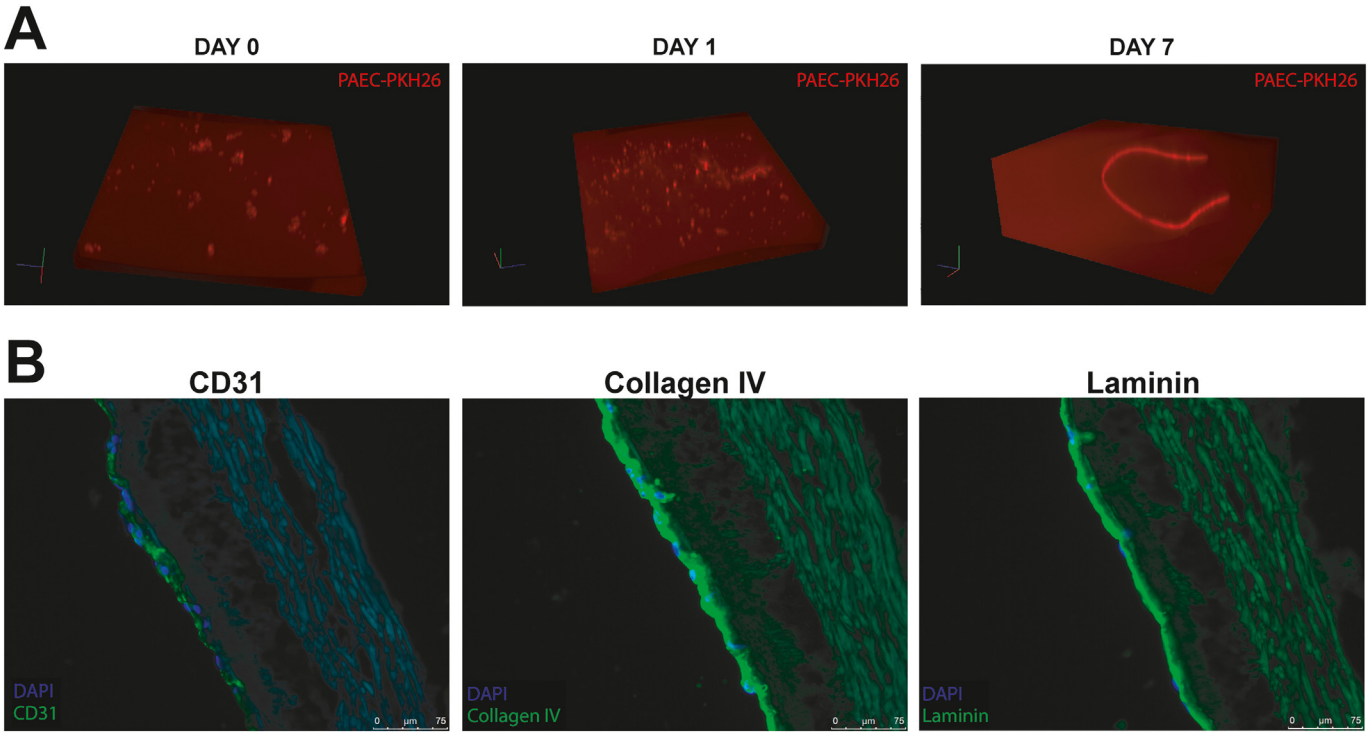

Fig. 5. In vitro biocompatibility testing and revascularization of decellularized porcine vascularized nerve grafts (pVNG-ECM). A) Representative 3D z-stack of recellularized pVNG-ECM at day 0 (immediately after injection into the vascular tree), day 1 and day 7 of cell culture under vascular flow using a spinning-disk confocal microscopy. wtPAEC were stained with PKH26 and seeded from the cannulated artery in the pVNG-ECM at day 0. Seeded grafts were maintained under flow for the next seven days. Cells started to form cell aggregates and groups on day 1 and elongated 3D structures were visible on day 7. B) Immunofluorescence staining of CD31, collagen type IV and laminin (green) and DAPI (blue) in re-endothelialized pVNG-ECM at day 7. Recellularization was observed in vessels that were in close proximity to the vascular pedicle, however no re-endothelialized capillaries in the periphery of the nerve were observed (one recellularization experiment representative of three). (For interpretation of the references to colour in this figure legend, the reader is referred to the web version of this article.)

was responsible for the primary undertaking, completion and supervision of all experiments. All authors interpreted data, revised manuscript and gave their final approval.

Funding source

The Study was supported partially by funds from the American Foundation for Surgery of the Hand [Award 1926 to EV and AT]. JD was funded by UCLouvain, Fondation Saint-Luc and Fonds Dr. Gaëtan Lagneaux. LM is a FNRS fellow.

Declaration of competing interest

The authors declare that they have no known competing financial interests or personal relationships that could have appeared to influence the work reported in this paper.

Acknowledgments

The authors thank the Experimental Surgery Facility of the University of Bern, Regula Buergy-Meyer for performing the critical point drying of the samples, Riccardo Sfriso for helping with the Nikon Eclipse Ti-E Spinning Disk microscope, Pascal Zürcher for help with the histology pictures and Alain Despont for his valuable and extensive support with the Luminex assays. This work was supported by the Microscopy Imaging Center (MIC), University of Bern.

References

[1] G. Davis, C.M. Curtin, Management of pain in complex nerve injuries, Hand Clin. 32 (2016) 257–262, https://doi.org/10.1016/j.hcl.2015.12.011.
[2] V. Chiono, C. Tonda-Turo, Trends in the design of nerve guidance channels in peripheral nerve tissue engineering, Prog. Neurobiol. 131 (2015) 87–104, https://doi.org/10.1016/j.pneurobio.2015.06.001.
[3] G.N. Panagopoulos, P.D. Megaloikonomos, A.F. Mavrogenis, The present and future for peripheral nerve regeneration, Orthopedics. 40 (2017) e141–e156, https://doi.org/10.3928/01477447-20161019-01.
[4] C.E. Schmidt, J.B. Leach, Neural tissue engineering: strategies for repair and regeneration, Annu. Rev. Biomed. Eng. 5 (2003) 293–347, https://doi.org/10.1146/annurev.bioeng.5.011303.120731.
[5] Y. Gao, Y.-L. Wang, D. Kong, B. Qu, X.-J. Su, H. Li, et al., Nerve autografts and tissue-engineered materials for the repair of peripheral nerve injuries: a 5-year bibliometric analysis, Neural Regen. Res. 10 (2015) 1003–1008, https://doi.org/10.4103/1673-5374.158369.
[6] X. Gu, F. Ding, D.F. Williams, Neural tissue engineering options for peripheral nerve regeneration, Biomaterials. 35 (2014) 6143–6156, https://doi.org/10.1016/j.biomaterials.2014.04.064.
[7] J. Du, H. Chen, L. Qing, X. Yang, X. Jia, Biomimetic neural scaffolds: a crucial step towards optimal peripheral nerve regeneration, Biomater Sci. 6 (2018) 1299–1311, https://doi.org/10.1039/c8bm00260f.
[8] W.P. Daley, S.B. Peters, M. Larsen, Extracellular matrix dynamics in development and regenerative medicine, J. Cell Sci. 121 (2008) 255–264, https://doi.org/10.1242/jcs.006064.
[9] D.A. Taylor, L.C. Sampaio, Z. Ferdous, A.S. Gobin, L.J. Taite, Decellularized matrices in regenerative medicine, Acta Biomater. 74 (2018) 74–89, https://doi.org/10.1016/j.actbio.2018.04.044.
[10] D.N. Brooks, R.V. Weber, J.D. Chao, B.D. Rinker, J. Zoldos, M.R. Robichaux, et al., Processed nerve allografts for peripheral nerve reconstruction: a multicenter study of utilization and outcomes in sensory, mixed, and motor nerve reconstructions, Microsurgery. 32 (2012) 1–14, https://doi.org/10.1002/micr.20975.
[11] B.D. Rinker, J.V. Ingari, J.A. Greenberg, W.P. Thayer, B. Safa, G.M. Buncke, Outcomes of short-gap sensory nerve injuries reconstructed with processed nerve allografts from a multicenter registry study, J. Reconstr. Microsurg. 31 (2015) 384–390, https://doi.org/10.1055/s-0035-1549160.
[12] B. Rinker, J. Zoldos, R.V. Weber, J. Ko, W. Thayer, J. Greenberg, et al., Use of processed nerve allografts to repair nerve injuries greater than 25 mm in the hand, Ann. Plast. Surg. 78 (2017) S292–S295, https://doi.org/10.1097/SAP.0000000000001037.
[13] N. Rbia, A.Y. Shin, The role of nerve graft substitutes in motor and mixed motor/sensory peripheral nerve injuries, J. Hand Surg. 42 (2017) 367–377, https://doi.org/10.1016/j.jhsa.2017.02.017.
[14] J. Isaacs, B. Safa, A preliminary assessment of the utility of large-caliber processed nerve allografts for the repair of upper extremity nerve injuries, Hand (N Y). 12 (2017) 55–59, https://doi.org/10.1177/1558944716646782.
[15] W.Z. Ray, S.E. Mackinnon, Management of nerve gaps: autografts, allografts, nerve transfers, and end-to-side neurorrhaphy, Exp. Neurol. 223 (2010) 77–85, https://doi.org/10.1016/j.expneurol.2009.03.031.
[16] J. Duisit, G. Orlando, D. Debluts, L. Maistriaux, D. Xhema, Y.-A.J. de Bisthoven, et al., Decellularization of the porcine ear generates a biocompatible, non-immunogenic extracellular matrix platform for face subunit bioengineering, Ann. Surg. 267 (2018) 1191–1201, https://doi.org/10.1097/SLA.0000000000002181.
[17] J. Duisit, L. Maistriaux, A. Taddeo, G. Orlando, V. Joris, E. Coche, et al., Bioengineering a human face graft: the matrix of identity, Ann. Surg. 1 (2017), https://doi.org/10.1097/SLA.0000000000002396.
[18] J. Duisit, H. Amiel, T. Wüthrich, A. Taddeo, A. Dedriche, V. Destoop, et al., Perfusion-decellularization of human ear grafts enables ECM-based scaffolds for auricular vascularized composite tissue engineering, Acta Biomater. 73 (2018) 339–354, https://doi.org/10.1016/j.actbio.2018.04.009.
[19] P. Muangsanit, R.J. Shipley, J.B. Phillips, Vascularization strategies for peripheral nerve tissue engineering, Anat. Rec. (Hoboken). 301 (2018) 1657–1667, https://doi.org/10.1002/ar.23919.
[20] J.K. Terzis, V.K. Kostopoulos, Vascularized nerve grafts and vascularized fascia for upper extremity nerve reconstruction, Hand (N Y). 5 (2010) 19–30, https://doi.org/10.1007/s11552-009-9189-4.
[21] S. D'Arpa, K.E.Y. Claes, F. Stillaert, B. Colebunders, S. Monstrey, P. Blondeel, Vascularized nerve "grafts": just a graft or a worthwhile procedure? Plast. Aesth. Res. 2 (2015) 183–194.
[22] C.A. Schneider, W.S. Rasband, K.W. Eliceiri, NIH image to ImageJ: 25 years of image analysis, Nat. Methods 9 (2012) 671–675.
[23] J. Schindelin, I. Arganda-Carreras, E. Frise, V. Kaynig, M. Longair, T. Pietzsch, et al., Fiji: an open-source platform for biological-image analysis, Nat. Methods 9 (2012) 676–682, https://doi.org/10.1038/nmeth.2019.
[24] S. Zhang, J. Shaw-Boden, Y. Banz, A.K. Bongoni, A. Taddeo, R. Spirig, et al., Effects of C1 inhibitor on endothelial cell activation in a rat hind limb ischemia-reperfusion injury model, J. Vasc. Surg. (2018), https://doi.org/10.1016/j.jvs.2017.10.072.
[25] L. Schaad, R. Hlushchuk, S. Barré, R. Gianni-Barrera, D. Haberthür, A. Banfi, et al., Correlative imaging of the murine hind limb vasculature and muscle tissue by MicroCT and light microscopy, Sci. Rep. 7 (2017) 41842, https://doi.org/10.1038/srep41842.
[26] A.K. Bongoni, J. Lanz, R. Rieben, Y. Banz, Development of a bead-based multiplex assay for the simultaneous detection of porcine inflammation markers using xMAP technology, Cytom. A. 83 (2013) 636–647, https://doi.org/10.1002/cyto.a.22287.
[27] R. Sfriso, S. Zhang, C.A. Bichsel, O. Steck, A. Despont, O.T. Guenat, et al., 3D artificial round section micro-vessels to investigate endothelial cells under physiological flow conditions, Sci. Rep. 8 (2018) 5898, https://doi.org/10.1038/s41598-018-24273-7.
[28] R. Sfriso, A. Bongoni, Y. Banz, N. Klymiuk, E. Wolf, R. Rieben, Assessment of the anticoagulant and anti-inflammatory properties of endothelial cells using 3D cell culture and non-anticoagulated whole blood, J Vis Exp. (2017) e56227, , https://doi.org/10.3791/56227.
[29] T.W. Gilbert, J.M. Freund, S.F. Badylak, Quantification of DNA in biologic scaffold materials, J. Surg. Res. 152 (2009) 135–139, https://doi.org/10.1016/j.jss.2008.02.013.
[30] A.B. Lovati, D. D'Arrigo, S. Odella, P. Tos, S. Geuna, S. Raimondo, Nerve repair using decellularized nerve grafts in rat models. A review of the literature, Front Cell Neurosci. 12 (2018) 427, https://doi.org/10.3389/fncel.2018.00427.
[31] C. Philips, F. Campos, A. Roosens, M. del Carmen Sánchez-Quevedo, H. Declercq, V. Carriel, Qualitative and quantitative evaluation of a novel detergent-based method for decellularization of peripheral nerves, Ann. Biomed. Eng. 46 (2018) 1921–1937, https://doi.org/10.1007/s10439-018-2082-y.
[32] M.W. McCrary, N.E. Vaughn, N. Hlavac, Y.H. Song, R.A. Wachs, C.E. Schmidt, Novel sodium deoxycholate-based chemical decellularization method for peripheral nerve, Tissue Eng. C Methods. 26 (2020) 23–36, https://doi.org/10.1089/ten.TEC.2019.0135.
[33] P.M. Crapo, T.W. Gilbert, S.F. Badylak, An overview of tissue and whole organ decellularization processes, Biomaterials. 32 (2011) 3233–3243, https://doi.org/10.1016/j.biomaterials.2011.01.057.
[34] World Health Organization. Recommendations for the Evaluation of Animal Cell Cultures as Substrates for the Manufacture of Biological Medicinal Products and for the Characterization…, n.d.
[35] CMC Information for Human Gene Therapy IND Applications, (n.d.). https://www.fda.gov/regulatory-information/search-fda-guidance-documents/chemistry-manufacturing-and-control-cmc-information-human-gene-therapy-investigational-new-drug.
[36] B. Ozlu, M. Ergin, S. Budak, S. Tunali, N. Yildirim, C. Erisken, A bioartificial rat heart tissue: perfusion decellularization and characterization, Int. J. Artif. Organs. 42 (2019) 757–764, https://doi.org/10.1177/0391398819863434.
[37] J.P. Guyette, S.E. Gilpin, J.M. Charest, L.F. Tapias, X. Ren, H.C. Ott, Perfusion decellularization of whole organs, Nat. Protoc. 9 (2014) 1451–1468, https://doi.org/10.1038/nprot.2014.097.
[38] M.J. Buckenmeyer, T.J. Meder, T.A. Prest, B.N. Brown, Decellularization techniques and their applications for the repair and regeneration of the nervous system, Methods. 171 (2019) 41–61, https://doi.org/10.1016/j.ymeth.2019.07.023.
[39] Y. Wakimura, W. Wang, S. Itoh, M. Okazaki, K. Takakuda, An experimental study to bridge a nerve gap with a decellularized allogeneic nerve, Plastic and Reconstructive Surgery 136 (2015) 319e–327e, https://doi.org/10.1097/PRS.0000000000001556.
[40] J. Valcarcel, R. Novoa-Carballal, R.I. Pérez-Martín, R.L. Reis, J.A. Vázquez, Glycosaminoglycans from marine sources as therapeutic agents, Biotechnol. Adv. 35 (2017) 711–725, https://doi.org/10.1016/j.biotechadv.2017.07.008.
[41] F. Bosse, Extrinsic cellular and molecular mediators of peripheral axonal regeneration, Cell Tissue Res. 349 (2012) 5–14, https://doi.org/10.1007/s00441-

012-1389-5.
[42] K. Belanger, T.M. Dinis, S. Taourirt, G. Vidal, D.L. Kaplan, C. Egles, Recent strategies in tissue engineering for guided peripheral nerve regeneration, Macromol. Biosci. 16 (2016) 472–481, https://doi.org/10.1002/mabi.201500367.
[43] S. Madduri, P. di Summa, M. Papaloïzos, D. Kalbermatten, B. Gander, Effect of controlled co-delivery of synergistic neurotrophic factors on early nerve regeneration in rats, Biomaterials. 31 (2010) 8402–8409, https://doi.org/10.1016/j.biomaterials.2010.07.052.
[44] S.L. Voytik-Harbin, A.O. Brightman, M.R. Kraine, B. Waisner, S.F. Badylak, Identification of extractable growth factors from small intestinal submucosa, J. Cell. Biochem. 67 (1997) 478–491.
[45] C.A. McDevitt, G.M. Wildey, R.M. Cutrone, Transforming growth factor-beta1 in a sterilized tissue derived from the pig small intestine submucosa, J. Biomed. Mater. Res. A 67 (2003) 637–640, https://doi.org/10.1002/jbm.a.10144.
[46] J.P. Hodde, D.M.J. Ernst, M.C. Hiles, An investigation of the long-term bioactivity of endogenous growth factor in OASIS Wound Matrix, J Wound Care 14 (2005) 23–25, https://doi.org/10.12968/jowc.2005.14.1.26721.
[47] J.L. Dziki, L. Huleihel, M.E. Scarritt, S.F. Badylak, Extracellular matrix bioscaffolds as immunomodulatory biomaterials, Tissue Eng Part A 23 (2017) 1152–1159, https://doi.org/10.1089/ten.TEA.2016.0538.
[48] X. Ren, P.T. Moser, S.E. Gilpin, T. Okamoto, T. Wu, L.F. Tapias, et al., Engineering pulmonary vasculature in decellularized rat and human lungs, Nat. Biotechnol. 33 (2015) 1097–1102, https://doi.org/10.1038/nbt.3354.
[49] E.M. Conway, P. Carmeliet, The diversity of endothelial cells: a challenge for therapeutic angiogenesis, Genome Biol. 5 (2004) 207, https://doi.org/10.1186/gb-2004-5-2-207.
[50] R. Marcu, Y.J. Choi, J. Xue, C.L. Fortin, Y. Wang, R.J. Nagao, et al., Human organ-specific endothelial cell heterogeneity, iScience 4 (2018) 20–35, https://doi.org/10.1016/j.isci.2018.05.003.